

Numerical Investigation of Copper Foam Adsorption Beds Packed with MOF-801 for Space Cooling and Desalination Applications

Mohamed Rezk ¹, Mahmoud B. Elsheniti ^{1,2}, Ahmed Rezk ^{1,3,4} and Osama A. Elsamni ¹

¹ Mechanical Engineering Department, Faculty of Engineering, Alexandria University, El-Chatby, Alexandria 21455, Egypt

² Mechanical Engineering Department, College of Engineering, King Saud University, Riyadh 11451, KSA.

³ Energy and Bioproducts Research Institute (EBRI), College of Engineering and Physical Science, Aston University, Birmingham, B4 7ET, UK.

⁴ Aston Institute of Material Research (AIMR), College of Engineering and Physical Science, Aston University, Birmingham, B4 7ET, UK

ABSTRACT

In this paper, an emerging Metal Organic Framework adsorbent MOF-801 packed into a recently developed copper foamed adsorbent-bed is numerically investigated under different operating conditions and physical parameters and benchmarked against the widely used silica gel adsorbent. A numerical model using lumped dynamic modelling approach was developed and validated against experimental data. An enhancement in the effective thermal conductivity for MOF-801 and silica gel foam packed bed and hence an improvement for the overall performance. The MOF-801-based system showed a higher performance for desalination application with a maximum production of specific daily water production of $13 \text{ m}^3/\text{ton}\cdot\text{day}$ compared to $9 \text{ m}^3/\text{ton}\cdot\text{day}$ for the silica gel-based system. MOF-801-based system evidenced its competition in the cooling application, achieving enhancement for the specific cooling power 140% higher than silica gel-based system.

Keywords: Adsorption, Desalination, cooling, MOF-801, Silica gel, Copper foam

NONMENCLATURE

Abbreviations

CC	Cooling Capacity (kW)
COP	The coefficient of performance
C_p	Specific heat capacity ($\text{J}/\text{kg}\text{ k}$)
D_{so}	Surface diffusivity pre-exponent constant (m^2/s)
E_a	Activation energy of surface diffusion (J/kg)
HTF	Heat transfer fluid

K	Thermal conductivity ($\text{W}/\text{m K}$)
$K_s a_v$	Overall mass transfer coefficient (s^{-1})
K_o	Pre-exponential constant in (Pa^{-1})
M	Mass (kg)
R_p	Adsorbent particle radius (m)
\bar{R}	Universal gas constant ($\text{J}/\text{kg K}$)
$\text{SCP}_{\cdot\text{mass}}$	Specific cooling power per unit mass ($\text{W}/\text{kg}_{\text{ads}}$)
$\text{SCP}_{\cdot\text{vol}}$	Specific cooling power per unit volume (kW/m^3)
SDWP	Specific daily water production ($\text{m}^3/(\text{ton}\cdot\text{day})$)
Sg	Silica gel
T	Temperature (K)
t	Time (s)
W	Specific adsorption ($\text{kg}/\text{kg}_{\text{ads}}$)
W_{eq}	Equilibrium adsorption uptake ($\text{kg}/\text{kg}_{\text{ads}}$)
<i>Symbols</i>	
ads	Adsorption
cond	Condenser
des	Desorption
evap	Evaporator
Hex	Heat exchanger
Ref	Refrigerant

1. INTRODUCTION

Nowadays, each of energy and fresh water resource faces rising demands and constraints in many regions of the world due to economic and population growth. It is predicted that around 52% of the world's population will face acute water scarcity by 2050 [1]. Freshwater scarcity leads to a greater reliance on alternative energy-intensive desalination systems (e.g., thermal, membrane and chemical desalination) to utilize brackish and

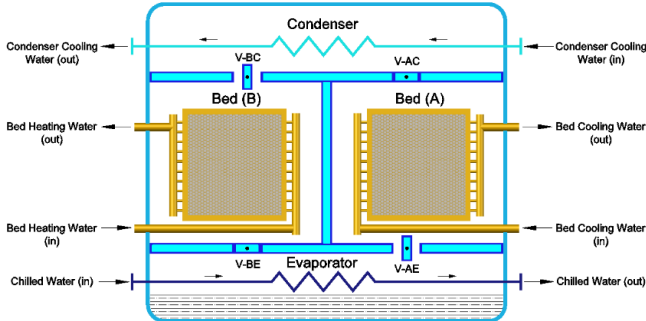


Fig. 1. Schematic diagram for the simulated adsorption chiller

seawater [2]. Besides, the current energy demand for space cooling tripled since 1990 [3]. Of the global energy consumption, the prospected share of space cooling share is almost 16% by 2050 [4]. Additionally, the widely spread conventional cooling systems utilize long-lasting ozone-depleting and global warming refrigerants [5].

Adsorption cooling and desalination systems are the most feasible alternatives utilizing low-grade heat sources (50 - 90 °C), such as solar and waste energy [6, 7]. In addition, adsorption cooling systems utilize eco-friendly working fluids, such as water, methanol and ethanol [8]. Nevertheless, such systems have the technical challenge of poor heat and mass transfer performance at the core component (i.e., adsorption bed) level, which leads to a relatively heavy and large physical footprint at the system level [9]. Also, the low COP, low SCP, and high initial cost hindered these systems from commercializing [10].

Many studies have been conducted to overcome these technical problems. Elsheniti et al. [11] investigated the impact of fin density on the overall performance of silica gel packed beds. It was concluded that quadrable fin density doubled the SCP_{mass}, reaching 305 W/kg_{ads}, while the system's maximum COP was 0.59 at 130 fins per tube. Askalany et al. [12] investigated the effect of using three different metallic additives materials (aluminium, copper and iron) with different concentrations from 10% to 30% of total mass to enhance the thermal conductivity of the granular activated carbon. Aluminium shows the highest effect on raising the thermal conductivity that using 30% aluminium fillings caused an increase in SCP_{mass} by 100% (from 0.015 kW/kg_{ads} to about 0.027 kW. /kg_{ads}) and a decrease in cycle time by 50%. Mohammed et al. [13] investigated experimentally and numerically the adsorption and desorption process of silica gel with different particles sizes packed into aluminium foam bed with various pores per inch (PPI) under typical operating conditions. Advanced system performance was

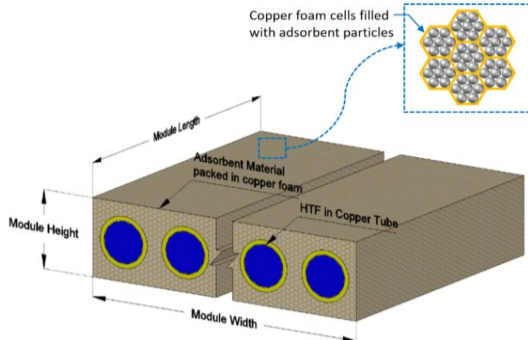


Fig. 2. Copper foam bed packed with adsorbent material with detailed copper foam cells filled with adsorbent particles reported; SCP_{mass} of 827 W/kg_{ads}, a SCP_{vol} of 517 W/m³ and a COP of 0.75 using 20 PPI aluminium foam.

Furukawa [14] investigated a group of zirconium MOFs materials and evaluated their performers based on three criteria: water condensation at low relative pressure, high water uptake capacity, and high recyclability and water stability. Among these materials was MOF-801, which showed an excellent performance with an uptake capacity of 22.5 wt % at P/P0 = 0.1. Solovyeva [15] has investigated MOF-801 for cooling application, which demonstrated COP and SCP_{mass} of 0.67 and 2000 W/kg_{ads}, respectively. Kim [16] proposed MOF-801 for water harvest with infiltration activated MOF-801 in a porous copper foam, improving the overall bed thermal conductivity and enhancing structural rigidity.

This work compares MOF-801 and silica gel, each packed into a copper foamed bed (i.e., MOF-801/copper foam and silica-gel/copper foam) for adsorption cooling and desalination applications. A numerical model using the Matlab platform was used to study the influence of the proposed bed materials on the overall system performance under typical operating conditions for cooling and desalination applications. Additionally, the influence of the operational and geometrical parameters was investigated by changing the operation cycle times at different bed heights.

2. SYSTEM DESCRIPTION

Fig 1 shows a schematic diagram for the simulated two-bed adsorption system. Typically, each adsorbent bed is connected to the evaporator or condenser by flap valves operated by the pressure difference between heat exchangers during adsorption/evaporation and desorption/condensation. Fig 2 illustrates the simulated adsorbent bed heat exchanger, consisting of plain copper tubes covered by rectangular copper foam packed with the adsorbent granules.

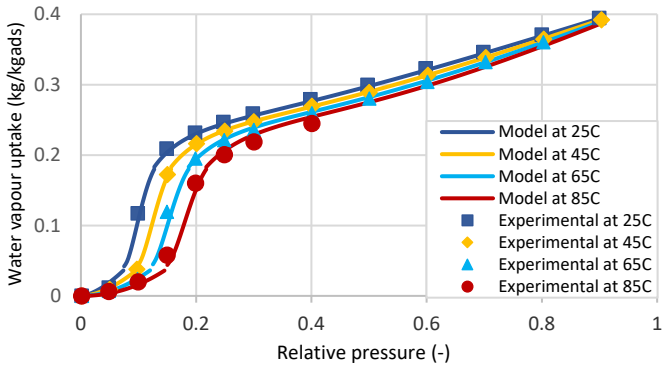


Fig. 3. Validation of proposed isotherm equations with the experimental data

2.1 Adsorption isotherm

The measured adsorption isotherms at temperatures (15 °C, 25 °C, 45 °C and 65 °C) [17] were fitted using series of exponential and polynomial characteristic equations (1)-(3).

$$w^* = 2.18865 * \exp(-6.61855669E - 4A) \quad (A > 6200) \quad (1)$$

$$w^* = 7.6163E - 11A^3 - 1.240E - 6A^2 + \quad (6200 \geq A) \quad (2)$$

$$6.5914E - 3A - 11.297 \quad \geq 4900 \quad (3)$$

$$w^* = -1.763E - 16A^4 - 1.2384E - 12A^3 + \quad (A < 4900) \quad (4)$$

$$2.2088E - 8A^2 - 1.0597E - 4A + 0.419$$

Where w^* is the uptake value at equilibrium conditions, and A is the adsorption potential, Eq. (4).

$$A = RT \ln \left(\frac{P}{P_s} \right) (0.002(T - 318)) + 1 \quad (4)$$

(P/P_s) denotes the evaporator/bed or condenser/bed pressure ratio during the adsorption and desorption process. The term ($0.002*(T-318)+1$) is a correlation factor for fitting the measured isotherms with the proposed equations. Fig. 3 shows the validation for the predicted characteristic equations for MOF-801.

2.2 Adsorption Kinetics

The linear driving force model (LDF) Eqs. (5)-(7), as per Sakoda and Suzuki were used to predict the rate of adsorption/desorption (dw/dt) using the temporal experimentally measured water fractional uptake curves [17].

$$\frac{dw}{dt} = k_s a_v (w^* - w) \quad (5)$$

$$k_s a_v = k_0 \exp \left(\frac{-E_a}{RT} \right) \quad (6)$$

$$k_0 = \frac{F D_{so}}{R_p^2} \quad (7)$$

The calculated kinetic parameters for MOF-801 are presented in this work, and the used parameters for silica gel from ref. [18] are furnished in Table 1. Fig. 4 shows the validation for the predicted kinetic curves parameters with the measured curves for MOF-801.

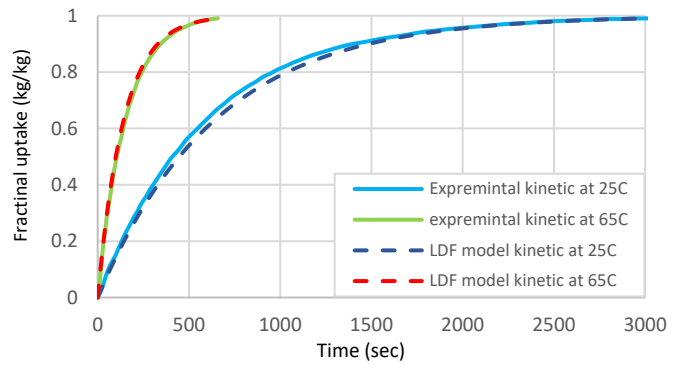


Fig. 4. Validation of proposed LDF kinetic parameters with the measured uptake curves at partial pressure 25%

Table 1

Linear driving force, LDF equation constants.

Symbol	MOF-801(This work)	Silica gel [18]	Unit
$F.D_{so}$	1.30558×10^{-10}	3.81×10^{-3}	m/s^2
E_a	3.1533×10^4	4.2×10^4	J/mol
R_p	5×10^{-7}	0.16×10^{-3}	m
k_0	522.23	2.939×10^6	s^{-1}

2.3 Adsorption chiller modeling.

It was assumed that: the adsorbent, adsorbate and heat exchanger metal are instantaneously at the same temperature, neglected heat and mass transfer to the surroundings. The energy balance equations for adsorption/desorption beds, evaporator and condenser are illustrated in Eqs. (8)-(10) [19].

$$\left(\xi M_{w,ads} C_{p,w}(T_{bed}) + M_{ads} w_{bed} C_{p,ref}(T_{bed}) + M_{ads} C_{p,ads} + M_{Hex,bed} C_{p,Hex,bed} \right) \frac{dT_{bed}}{dt} = (\phi, \delta) M_{ads} \frac{dw_{bed}}{dt} [\gamma \{ h_g(T_{Hex}) - h_g(P_{Hex}, T_{bed}) \} + (1-\gamma) \{ h_g(P_{Hex}, T_{bed}) - h_g(P_{bed}, T_{bed}) \}] + \sum_{n=1}^{N_{bed}} \phi M_{ads} \frac{dw_{bed}}{dt} \Delta H_{ads} + (1-\xi) \sum_{n=1}^{N_{bed}} dU A_{bed,k} \times LMTD_{bed} \quad (8)$$

$$C_{p,ref,f}(T_{evap}) M_{ref,evap} + M_{Hex,evap} C_{p,Hex,evap} \frac{dT_{evap}}{dt} = U A_{evap} \times LMTD_{evap} + \frac{d}{dt} E_{pump} \phi M_{ads} \frac{dw_{bed}}{dt} [(h_{ref,evap,in} - h_{ref,evap,out})] \quad (9)$$

$$C_{p,ref,l}(T_{cond}) M_{ref,cond} + M_{Hex,cond} C_{p,Hex,cond} \frac{dT_{cond}}{dt} = U A_{cond} \times LMTD_{cond} + \phi M_{ads} \frac{dw_{bed}}{dt} [(h_{ref,cond,in} - h_{ref,cond,out})] + C_{p,ads}(T_{cond} - T_{bed}) \quad (10)$$

2.4 Bed thermal resistance

Fig 5 (A) shows a control volume of an incremental element from the adsorber bed. Each element consists of a copper tube surrounded by adsorbent material/copper foam. Fig. 5 (B) presents a schematic diagram for the bed heat transfer resistances during the heat transfer from/to the heat transfer fluid (HTF) to/from the surrounded vapor during

desorption/adsorption modes. There are five heat transfer resistances: (R1) radial convection thermal resistance from the HTF fluid stream to the internal tube wall, (R2) radial conduction thermal resistance through the tube wall, (R3) contact thermal resistance between the adsorbent material and tube outside surface and (R4 and R5) two conduction thermal resistances through the adsorbent material in radial and axial direction respectively. The incremental axial conduction thermal resistance through the tube wall was neglected due to its insignificant effect compared to other resistances.

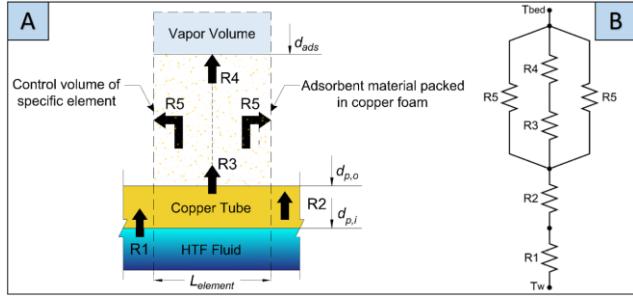


Fig. 5. Validation of proposed LDF kinetic parameters with the measured uptake curves at partial pressure 25%

The mathematical formula of the heat transfer resistance is illustrated in Table 2. htc , A , d , k , R_{cont} and $L_{element}$ denote the convection heat transfer coefficient, surface area, diameter, thermal conductivity, contact thermal resistance and adsorbent element thickness, respectively. Subscripts i, o, t, and ads refer to inside, outside, tube, and adsorbent.

Table 2

Mathematical formula of bed heat transfer resistances.

Resistance	Value
R_1	$\frac{1}{htc_{i,bed}A_{i,bed}}$
R_2	$\frac{\ln(d_{p,o} - d_{p,i})}{2\pi k_t L_{element}}$
R_3	$\frac{R_{cont}}{\pi d_o L_{element}}$
R_4	$\frac{\ln(\frac{d_{ads}}{d_{p,o}})}{2\pi k_{ads} L_{element}}$
R_5	$\frac{(\frac{L_{element}}{2})}{A_{ads} k_{ads}}$

3. RESULTS

The influence of changing the operational and geometrical parameters on the overall performance for the adsorption cooling and desalination systems with using MOF-801/copper foam comparing to silica-gel/copper foam as adsorption materials were investigated. The effect of the cycle time on the

operation performance was studied from 200 s to 1000 s at different bed heights from 20 mm to 32 mm. Fig. 6 to Fig. 9 shows the impact of the cycle time and bed height on the SDWP, CC, SCP_{mass} and SCP_{vol} for both materials. The heating, cooling and chilled water temperatures were kept constant at 85 °C, 30 °C and 15 °C respectively.

3.1 The water and cooling production (SDWP and CC)

Fig. 6 shows that the SDWP for the MOF-801 outperforming silica gel at all cycle times and bed heights. The maximum SDWP for both materials occurs at bed height 20 mm to be 13 m³/(ton.day) for MOF-801 at cycle time 300 s compared to 9 m³/(ton.day) for silica gel at cycle time 200 s. The outperforming performance of the MOF-801 for water production stemmed from its steep isotherm curve, which increases its cycling adsorption uptake compared to silica gel at the same cycle times, as shown in Fig. 10. Referring to the difference of the packing densities between the two materials, the mass of MOF-801 equals 48.78 kg compared to 67.95 kg for silica gel at same bed size. Despite this mass difference, the CC for MOF-801 exceeded silica gel at most operation conditions, as shown in Fig. 7. It is noted that the gap of CC between MOF-801 and silica gel is decreasing with the decreasing of cycle times and the increasing of bed height which makes the CC for the silica gel exceed MOF-801 at cycle times below 400 s for bed heights from 20 mm to 24 mm. The maximum CC for both materials achieved at bed height 32 mm to be 16 kW at cycle time 400 s for MOF-801 and 15.2 kW at cycle time 300 s for silica gel.

3.2 The specific cooling powers per unit mass and per unit volume (SCP_{mass} and SCP_{vol})

Fig. 8 shows that SCP_{mass} for MOF-801 outperforming silica gel at all cycle times and bed heights owing to the high cyclic uptake capacity for MOF-801 compared to silica gel. The maximum SCP_{mass} achieved at bed height 20 mm to be 365 W/kg for MOF-801 at cycle time 300 s compared to 260 W/kg for silica gel at cycle time 200 s.

As shown in Fig. 9, the SCP_{vol} for MOF-801 exceeded silica gel at cycle times more than 400 s for all bed heights. Notably, the increase of the SCP_{vol} for silica gel is more rapidly with the decreasing cycle times compared to MOF-801, which makes the SCP_{vol} for the silica gel exceed MOF-801 at cycle time 200 s and bed heights less than 28 mm. The maximum SCP_{vol} occurs for both materials at bed height 20 mm, reaching 185 kW/m³ for silica gel at cycle time 200 s and 170 kW/m³ for MOF-801 at cycle time 300 s.

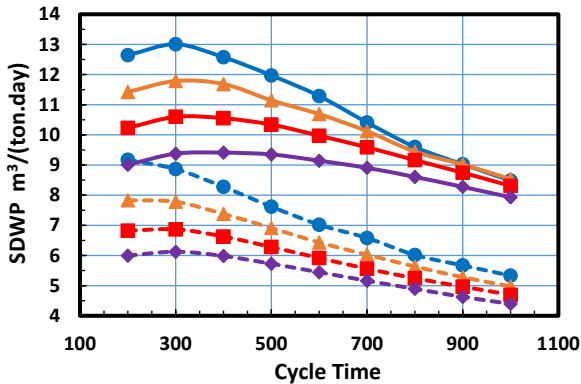


Fig. 8. MOF-801 and Silica-gel each with copper foam (SDWP)

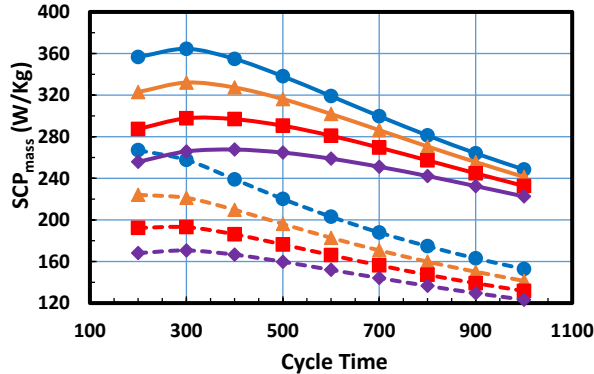


Fig. 10. MOF-801 and Silica-gel each with copper foam (SCP_{mass}) Fig. 11. MOF-801 and Silica-gel each with copper foam (SCP_{vol})

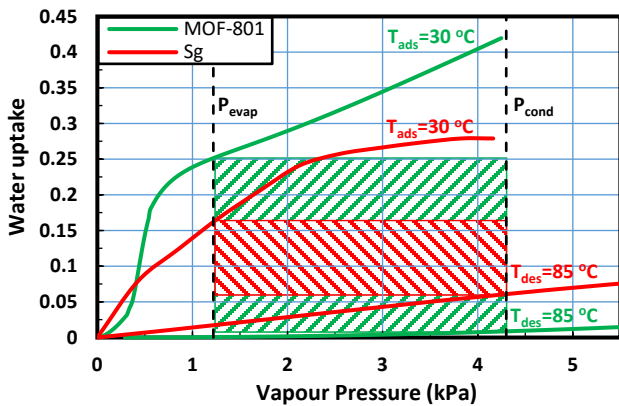
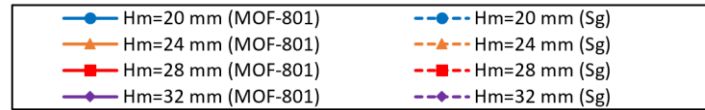


Fig. 7. Isotherms comparison with ideal cycle superimposed

3.3 The Coefficient of performance (COP)

Decreasing bed heights showed a more significant influence on the COP of silica gel compared to MOF-801. The COP of silica gel outperforming MOF-801 for cycle times more than 400 s at all bed heights, as shown in Fig. 11. For low cycle times as in 200 s, the COP of MOF-801 exceeds silica gel for bed height more than 24 mm. The maximum COP for silica gel and MOF-801 is 0.76, 0.7 occurred at cycle time 1000 s and bed height 20 mm.

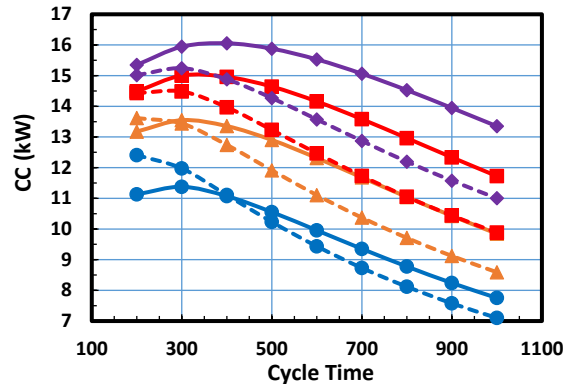


Fig. 9. MOF-801 and Silica-gel each with copper foam (CC)

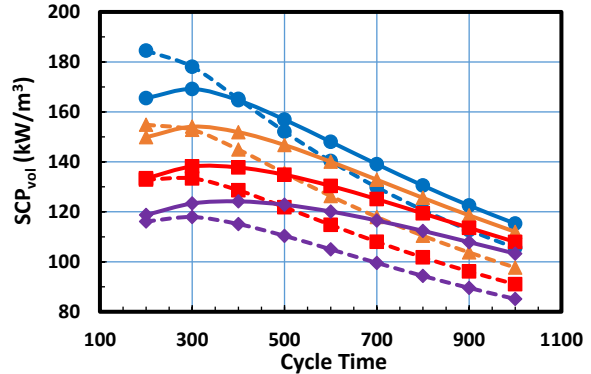


Fig. 11. MOF-801 and Silica-gel each with copper foam (SCP_{vol})

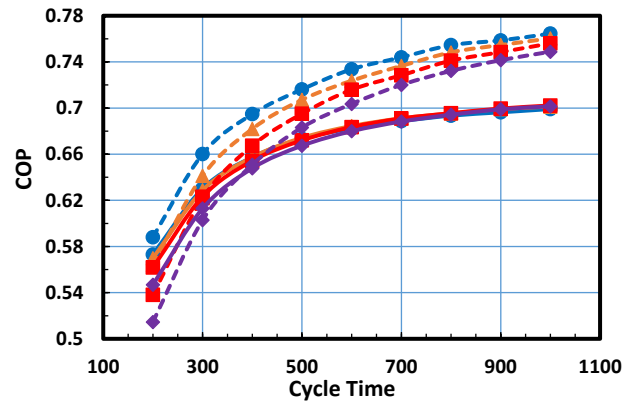
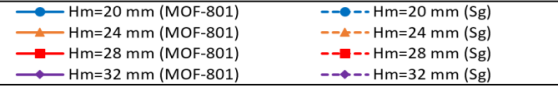


Fig. 6. MOF-801 and Silica-gel each with copper foam (COP)



4. CONCLUSION

This study compared MOF-801 and silica gel packed into a newly developed copper foamed bed for adsorption cooling and desalination applications. In addition, the influence of changing the cycle times and bed heights on the operation performance were investigated. The following conclusions were drawn:

- 1- The contribution of the copper foams significantly influenced the bed thermal conductivity and improved the over operation performance for both materials.
- 2- MOF-801 outperformed silica gel in water desalination applications, achieving a maximum SDWP of $13 \text{ m}^3/(\text{ton}\cdot\text{day})$ compared to $9 \text{ m}^3/(\text{ton}\cdot\text{day})$ for the silica gel.
- 3- MOF-801 evidence its capability for cooling applications compared to silica gel with maximum SCP_{mass} and SCP_{vol} of 365 W/kg and 170 kW/m³ compared to 260 W/kg and 185 kW/m³ for silica gel.
- 4- Silica gel achieved a higher COP than MOF-801 at the cycle times more than 400 s for all studied bed heights with a maximum COP of 0.76 for silica gel compared to 0.7 for MOF-801 at cycle time 1000 s.

REFERENCE

- [1] UNESCO. UN-Water, United Nations World Water Development Report 2020: Water and Climate Change, Paris. 2020; Available from: <https://www.unwater.org/publications/world-water-development-report-2020/>.
- [2] IEA (International Energy Agency). Introduction to the water-energy nexus, IEA, Paris 2020; Available from: <https://www.iea.org/articles/introduction-to-the-water-energy-nexus>.
- [3] IEA (International Energy Agency). Cooling, IEA, Paris 2020; Available from: <https://www.iea.org/reports/cooling>.
- [4] IEA (International Energy Agency). The Future of Cooling, IEA, Paris 2018; Available from: <https://www.iea.org/reports/the-future-of-cooling>.
- [5] Calm, J., Emissions and environmental impacts from air-conditioning and refrigeration systems. International Journal of Refrigeration, 2002. 25: p. 293-305.
- [6] Alsaman, A.S., et al., Performance evaluation of a solar-driven adsorption desalination-cooling system. Energy, 2017. 128: p. 196-207.
- [7] Ng, K., et al., Study on a waste heat-driven adsorption cooling cum desalination cycle. International Journal of Refrigeration-revue Internationale Du Froid - INT J REFRIG, 2012. 35.
- [8] Chekirou, W., et al., Dynamic modelling and simulation of the tubular adsorber of a solid adsorption machine powered by solar energy. Int J Refrig, 2014. 39: p. 137-151.
- [9] Smith, D.S., et al., Thermal conductivity of porous materials. Journal of Materials Research, 2013. 28(17): p. 2260-2272.
- [10] ul Qadir, N., S.A.M. Said, and R.B. Mansour, Modeling the performance of a two-bed solar adsorption chiller using a multi-walled carbon nanotube/MIL-100(Fe) composite adsorbent. Renewable Energy, 2017. 109: p. 602-612.
- [11] Elsheniti, M.B., M.A. Hassab, and A.-E. Attia, Examination of effects of operating and geometric parameters on the performance of a two-bed adsorption chiller. Applied Thermal Engineering, 2019. 146: p. 674-687.
- [12] Askalany, A.A., et al., Effect of improving thermal conductivity of the adsorbent on performance of adsorption cooling system. Applied Thermal Engineering, 2017. 110: p. 695-702.
- [13] Mohammed, R.H., et al., Performance enhancement of adsorption beds with silica-gel particles packed in aluminum foams. International Journal of Refrigeration, 2019. 104: p. 201-212.
- [14] Furukawa, H., et al., Water Adsorption in Porous Metal-Organic Frameworks and Related Materials. Journal of the American Chemical Society, 2014. 136(11): p. 4369-4381.
- [15] Solovyeva, M.V., et al., MOF-801 as a promising material for adsorption cooling: Equilibrium and dynamics of water adsorption. Energy Conversion and Management, 2018. 174: p. 356-363.
- [16] Kim, H., et al., Water harvesting from air with metal-organic frameworks powered by natural sunlight. Science, 2017. 356(6336): p. 430-434.
- [17] Kim, H., et al., Adsorption-based atmospheric water harvesting device for arid climates. Nature Communications, 2018. 9(1).
- [18] Rezk, A., et al., Characterisation of metal organic frameworks for adsorption cooling. International Journal of Heat and Mass Transfer, 2012. 55(25): p. 7366-7374.
- [19] Rezk, A., et al., Effects of contact resistance and metal additives in finned-tube adsorbent beds on the performance of silica gel/water adsorption chiller. Applied Thermal Engineering, 2013. 53(2): p. 278-284.